Two Simple and Highly Efficient Variants of the Griffith-Ley Oxidation of Alcohols

Pascal Weingart,[a] Patrick Hütchen,[a] Angelo Damone,[b] Maximilian Kohns,[b] Hans Hasse,[b] and Werner R. Thiel*[a]

The Griffith-Ley oxidation of alcohols to aldehydes and ketones is performed with either $RuCl_3 \cdot (H_2O)_x$ or a highly stable, well-defined ruthenium catalyst and with cheap trimethylamine *N*-oxide (TMAO) as the oxygen source. The use of *n*-heptane as the solvent, which forms a second phase with TMAO and a part of the alcohol, allows the reactions to be performed with a minimum amount of catalyst. This results in high local concentrations and thus to very rapid conversions. Detailed quantum chemical calculations suggest, that the Griffith-Ley oxidation not necessarily requires high oxidation states of ruthenium but can also proceed with Ru^{II}/Ru^{IV} species.

Introduction

Historically, stoichiometric quantities of hazardous chromium (VI) or manganese(VII) compounds were used to oxidize alcohols to ketones and aldehydes.[1] This changed in 1987 when W. P. Griffith and co-workers found that tetraalkylammonium perruthenate(VII) in combination with *N*-methylmorpholine *N*-oxide converts alcohols into the corresponding ketones and aldehydes in a highly selective manner.[2] Since this reaction is rather tolerant to functional groups and requires only low concentrations of the catalyst, it has reached widespread applications in organic synthesis.[3]

However, the history of this reaction dates back to 1976, when Sharpless and co-workers published a rarely cited short communication wherein they described the performance of a series of ruthenium compounds and different *N*-oxides in the oxidation of alcohols.[4] In contrast to the 1987 report of Griffith, the authors focused on ruthenium species in the oxidation states 0-IV. Some of them were inactive such as $(RuO_2 \cdot (H_2O)_x$, $Ru(acac)_3$, $RuCl_3(NO)(PPh_3)_2$) but others like $RuCl_2(PPh_3)_3$, $Ru_3(CO)_{12}$ and $RuCl_3 \cdot (H_2O)_x$ showed rather good activities. The reactions were performed in acetone or DMF at room temperature and gave yields between 65 and 100% after a reaction time of 2 h with a catalyst loading of 0.84 mol% and two equiv. of *N*-methylmorpholine *N*-oxide. Only a few alcohols (cholesterol, 1-nonen-4-ol, β-3-indolylethanol) turned out to be unreactive under the given conditions. The authors also investigated the use of other *N*-oxides than *N*-methylmorpholine *N*-oxide but stated that the reactions stopped at yields between 40 and 70% with these oxygen sources. Pyridine *N*-oxide and some of its derivatives turned out to be inactive.

In their work Sharpless and co-workers pointed out that "The mechanism of these oxidations probably involves formation of a ruthenium alkoxide which undergoes β-elimination to produce the carbonyl compound and a ruthenium hydride. The ruthenium hydride (or its equivalent) could be oxidized by the amine-*N*-oxide and then the cycle could be repeated."[4a] According to this, the reaction can be considered at least partially as a reversion of a transfer hydrogenation of ketones or aldehydes. Bäckvall et al. proved that a transfer dehydrogenation of alcohols is in principle possible with acetone as the hydrogen acceptor and $(PPh_3)_3RuCl_2$ or Shvo's catalyst.[5] In contrast to this, high reaction states were postulated in the literature to drive the Griffith-Lay oxidation.[2,6]

In course of a study on the oxidation of alcohols from natural resources, we were looking for catalyst systems giving optimum yields and selectivities in the dehydrogenation of alcohols to aldehydes and ketones in the presence of a reasonably priced oxidizing agent. We therefore revived the protocol of Sharpless and co-workers under these basic conditions. In addition, we wanted to elucidate by means of quantum chemical calculations whether the Sharpless concept of a mechanism based on ruthenium species in low oxidation states is energetically possible.

Accordingly, the manuscript is structured in two sections, one focusing on the experiments carried out to optimize catalyst and reaction conditions and a second one which is devoted to DFT calculations.

[a] *P. Weingart, P. Hütchen, Prof. W. R. Thiel*
Fachbereich Chemie
Technische Universität Kaiserslautern
Erwin-Schrödinger-Str. 54
67663 Kaiserslautern (Germany)
E-mail: thiel@chemie.uni-kl.de
[b] *Dr. A. Damone, Prof. M. Kohns, Prof. H. Hasse*
Lehrstuhl für Thermodynamik
Fachbereich Maschinenbau und Verfahrenstechnik
Technische Universität Kaiserslautern
Erwin-Schrödinger-Str. 44
67663 Kaiserslautern (Germany)

Supporting information for this article is available on the WWW under https://doi.org/10.1002/cctc.202000413

This publication is part of a joint Special Collection with EurJIC on "Pincer Chemistry & Catalysis". Please follow the link for more articles in the collection.

Results and Discussion

Catalysis

Since $RuCl_3 \cdot (H_2O)_x$ is by far the cheapest source of ruthenium available, it was the catalyst of choice from the very beginning. Sharpless and co-workers reported that $RuCl_3 \cdot (H_2O)_x$ was approx. 20% less active than $RuCl_2(PPh_3)_3$ and $Ru_3(CO)_{12}$. However, the costs for $RuCl_3 \cdot (H_2O)_x$ are by a factor of six lower than for tetraalkylammonium perruthenate(VII) and by factor of five lower than for $RuCl_2(PPh_3)_3$ based on the ruthenium content. $Ru_3(CO)_{12}$ has almost the same price as $RuCl_3 \cdot (H_2O)_x$ but the latter one is much simpler to handle. Concerning the cost of the *N*-oxide, pyridine *N*-oxide is the cheapest. We therefore reinvestigated the application of this *N*-oxide under the conditions of Sharpless and found low reactivity as reported. In addition, other low-prized oxygen sources such as acetone (Oppenauer-type oxidation), dioxygen, hydrogenperoxide and TBHP (*tert*-butylhydroperoxide) gave no conversion. Among the *N*-oxides with sp^3-hybridized nitrogen atoms, trimethylamine *N*-oxide (TMAO) dihydrate is the cheapest relative to the molecular mass. Highly volatile trimethylamine would be the sole by-product, which can easily be recovered and in principle be reoxidized to TMAO in processes larger than lab-scale experiments.

TMAO is well known for the in-situ activation of catalysts by oxidative decarbonylation of metal carbonyl complexes.[7] However, it has hardly been investigated as an alternative hydrogen acceptor resp. oxygen donor in catalytic oxidation reactions so far. In 1990, Maumy et al. published a copper mediated oxidation of benzylic alcohols with TMAO as the oxygen source.[8] It proceeds with copper alcoholates that have to be performed in-situ. Good yields of the corresponding aldehydes and ketones are obtained in the presence of four equivalents of TMAO. In 1997, Ley and co-workers reported the oxidation of alcohols with TMAO with 20 mol% of a polymer supported perruthenate reagent as a heterogeneous catalyst.[9] In the presence of molecular sieves and 1.0 equiv. of TMAO they were able to convert 1-phenylethanol to acetophenone within 18 h at room temperature in 60% yield. Pearson and co-workers published in 2005 the first iron catalyzed oxidation of alcohols with TMAO as the hydrogen acceptor.[10] They reported the oxidation of various allylic and benzylic alcohols by using 30 mol% of (η^4-cyclohexadiene)$Fe(CO)_3$ as the catalyst with 3.0 equiv. of TMAO in benzene at room temperature. Substrate conversions varied between 87% and 98% after 10 h of reaction time. In the year 2012, Woo and co-workers were the first to report a gold catalyzed oxidative dehydrogenation of dibenzylamine using TMAO as the oxidant.[11] By reacting 1 mmol of pure gold powder and 0.066 mmol of TMAO with 0.012 mmol of Bn_2NH they could reach 77% of the imine product within 24 h in CD_3CN at 60 °C.

With $RuCl_3 \cdot (H_2O)_x$ as the catalyst, 1-phenylethanol as the substrate and TMAO as the oxygen source, a short series of experiments was carried out to optimize the reaction conditions (Table 1). Among all solvents that were tested, DMF gave the best results.

Table 1. Evaluation of the reaction conditions for the oxidation of 1-phenylethanol with $RuCl_3 \cdot (H_2O)_x$ as the catalyst.[a]

Entry	Cat. [mol%]	Equiv. TMAO	Temp. [°C]	Yield [%][b] After t [min] 10	30	60
1	0.5	2 [c]	60	26	30	40
2	0.5	3	80	98	98	98
3	0.5	2	80	76	78	79
4	0.5	1.1	80	59	59	59
5	0.5	3	60	>99	>99	>99
6	0.5	2	60	95	96	96
7	0.5	1.1	60	64	65	67
8	0.5	3	40	97	>99	>99
9	0.5	2	40	84	89	90
10	0.5	1.1	40	57	62	63

[a] Reaction conditions: 1-phenylethanol (1 mmol), 1 mL of DMF, 100 µL of tetradecane (internal standard); [b] yields determined by GC; [c] with $TMAO \cdot (H_2O)_2$ instead of TMAO.

Entry 1 (Table 1) shows, that the presence of larger amounts of water are detrimental for the performance of the process, since the use of $TMAO \cdot (H_2O)_2$ distinctly reduces the yield of the product. The dihydrate is much cheaper than pure TMAO, but there is no problem to remove the water by azeotropic distillation with toluene or DMF.[12] The most important information that can be drawn from Table 1 is, that there must be a temperature dependent deactivation process with $RuCl_3 \cdot (H_2O)_x$ as the catalyst. Comparing entries 2 and 5 or entries 3 and 6 clearly proves this statement: The yield of acetophenone is higher at the lower temperatures. A further decrease of the reaction temperature to 40 °C (entry 8) then leads to a slightly poorer yields. Table 1 makes clear, that the deactivation process is rapid, since there is almost no improvement of the yield after 10 min of reaction time. However, the oxidation process at lower temperatures must therefore be even faster than the deactivation, otherwise high yields would not be feasible.

For the evaluation of the substrate scope, the conditions of entry 5 in Table 1 were applied. Samples were taken after 10 min of reaction time. Scheme 1 summarizes the results.

Performing the reaction in an alkane as the solvent instead of DMF would simplify the product separation at the end of the reaction. For this, we applied ruthenium complex **1** (Scheme 2), which we recently developed for the transfer hydrogenation of ketones, aldehydes and imines.[13] Compound **1** is highly active in these conversions.

Since Sharpless et al. postulated the ruthenium catalyzed oxidation of alcohols to ketones resp. aldehydes with *N*-oxides to be a reversion of the transfer hydrogenation,[4] it seemed worth to investigate compound **1** for the oxidation reaction, too. In addition, there are no other oxidizable ligands in **1** than the phosphine ligand, which speaks for a structural motif that should be rather stable under the reaction conditions.

According to the butyl and allyl substituents of its ligand, it is well soluble in almost all organic solvents, only in non-polar hydrocarbons it is sparingly soluble. Since TMAO is only poorly soluble in alkanes too, the ternary mixture of TMAO, *n*-heptane and the substrate separates in a two-phase system with a tiny amount of a polar phase, having the red color of catalyst **1**.

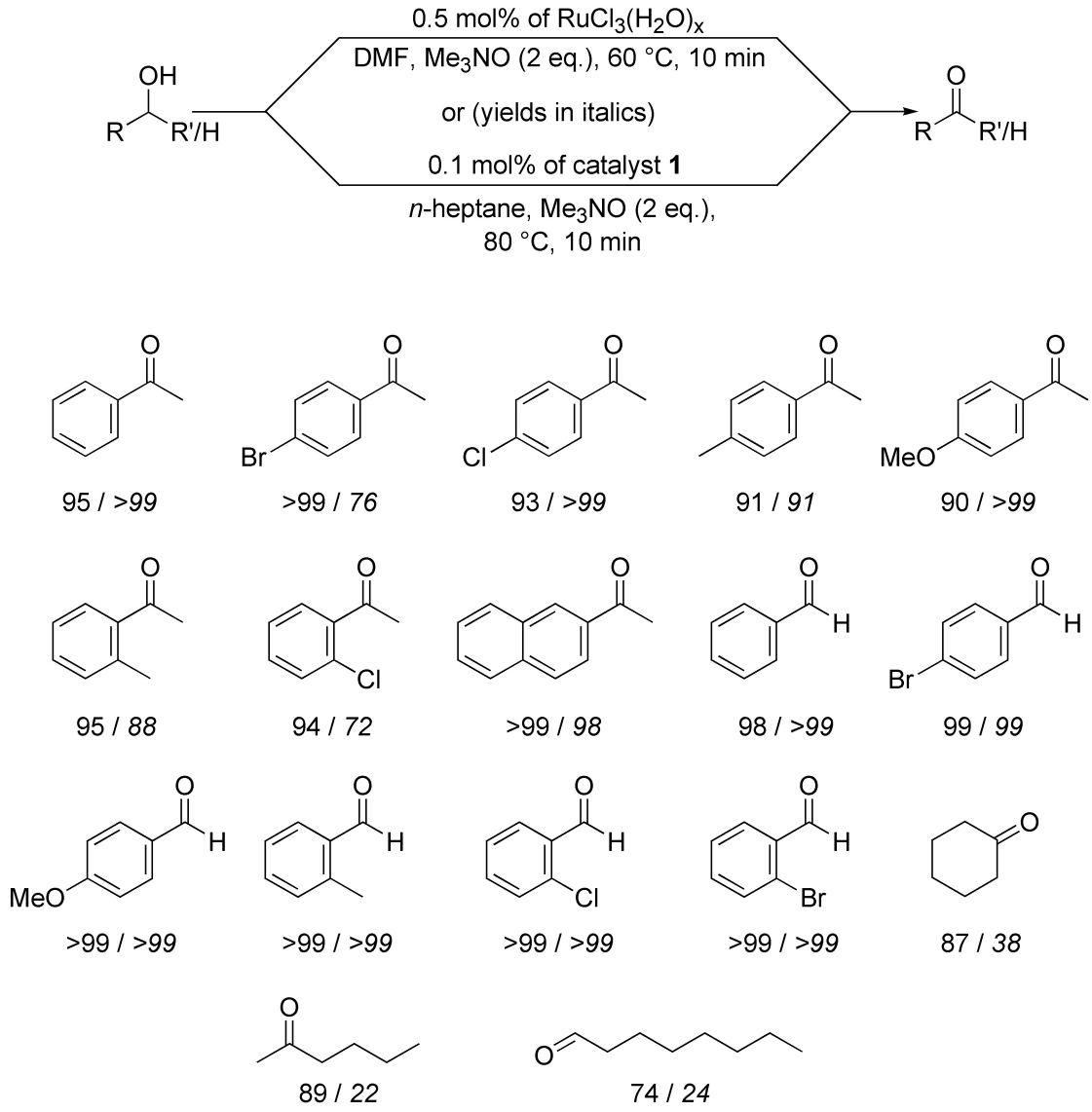

Scheme 1. Carbonyl products derived from alcohol oxidation. The yields were determined by GC and the reaction time was 10 min in all cases. Reaction conditions: substrate (1 mmol), 0.5 mol% of $RuCl_3 \cdot (H_2O)_x$ or 0.1 mol% of **1**, Me_3NO (2 eq.), DMF (1 mL) or *n*-heptane (3 mL, yields in italics), 100 μL of tetradecane (internal standard), 60 or 80 °C.

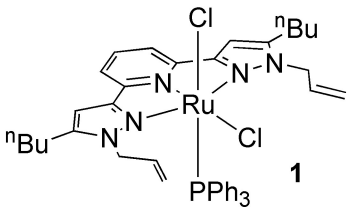

Scheme 2. Molecular structure of catalyst **1**.

According to the solubilities in polar/non-polar solvents of the components taking part in the catalysis it seems reasonable to assume that most of the TMAO and a part of the alcohol will combine together with catalyst **1** in this second phase. If this is true, the catalyst is surrounded by high local concentrations of the oxidizing agent and the alcohol, which explains the very high conversions even with catalyst loadings being as low as 0.1 mol% (Scheme 1). At the end of the reaction, the tiny droplets containing the main amount of the catalyst still show the typical strawberry-red color of catalyst **1**. Obviously aliphatic alcohols give poorer results with **1** as the catalyst than aromatic ones. Here, the second polar phase is not formed, since these substrates are well soluble in *n*-heptane. To prove this theory, a small amount (200 μL) of DMF was added to create the second polar phase. This leads to distinctly higher yields of carbonyl compounds (cyclohexanone, 46; 2-hexanone, 47; octanal, 48%). Prolonging the reaction time to 30 min for the aliphatic substrates does not further improve the outcome of the reaction. Recovering the polar phase by decantation of the heptane phase allows a reuse of the catalyst. After filling the

vial with another charge of *n*-heptane, internal standard, TMAO and 1-phenylethanol, still a conversion of about 50% could be achieved. It has to be mentioned here, that some water is formed during the first experiment, which is known to hamper complete conversions. This was not removed from the polar phase.

DFT calculations

To get a deeper insight in the mechanism, quantum chemical calculations including a solvent model for DMF were carried out with a model species **A** (Scheme 3) which is structurally closely related to catalyst **1**. We left the *n*butyl groups and changed the allylic side chains into methyl groups to facilitate the search for energetic minima. Ethanol was taken as the model alcohol, since the oxidation of primary aliphatic alcohols resulting in aldehyde formation is harder to achieve than the oxidation of secondary alcohols leading to ketones or primary benzylic alcohols. The calculated barriers can therefore be considered as are an upper bound for other substrates.

In order to simplify the entrance into the mechanistic discussion, we have divided the presentation of our results in four parts that are summarized in Scheme 3 in a shortened form. They will be discussed below in more detail. The catalytic cycle of the alcohol oxidation starts with the catalyst activation and ends up with the catalyst regeneration. For the actual oxygen transfer, two alternative mechanistic routes, the oxo and the hydrido pathway, were found, both including a $Ru^{II} \rightarrow Ru^{IV} \rightarrow Ru^{II}$ sequence but differing in their elemental steps. After the activation of catalyst **A**, which ends with the chloridoethanolatoruthenium(II) intermediate **E**, the oxo pathway follows the addition of TMAO and the formation of a ruthenium(IV) oxo species. It is completed with the abstraction of a β-hydrogen atom from the alcoholato ligand and the dissociation of acetaldehyde. β-Hydrogen abstraction is in contrast the first step in the hydrido pathway where it is followed by the generation of a hydridooxoruthenium(IV) species. This pathway is completed by a 1,2-hydrogen shift leading to the same hydroxochloridoruthenium(II) species **I** as the oxo pathway. Regeneration of **E** proceeds via an OH/OEt exchange. The overall oxidation of ethanol to acetaldehyde according to Scheme 3 was calculated to be exothermic by $\Delta H = -38.61$ kcal/mol and exergonic by $\Delta G = -53.42$ kcal/mol. The four parts of the calculated mechanism shall in the following be discussed in more detail.

Catalyst activation. For binding any substrate, a free coordination site has to be generated at the ruthenium centre. Therefore, the activation of **A** starts with the dissociation of triphenylphosphine, which is endothermic by +8.37 but exergonic by −11.21 kcal/mol (Figure 1). These values are calculated without the presumably occurring, exothermic oxidation of triphenylphosphine in the presence of trimethylamine *N*-oxide. In the intermediate 16VE ruthenium(II) complex **Ba** the two chlorido ligands end up in *trans*-geometry. An isomer **Bb** wherein the two chlorido ligands are found in *cis*-orientation to each other (one chlorido ligand in *trans*-position to the pyridine donor) was calculated to be another local minimum and is approx. 7 kcal higher in energy than **Ba** (see the Supporting Information). Due to the low difference in energy between **Ba** and **Bb**, we calculated both isomers **Ca** and **Cb** that are formed by addition of ethanol. Isomer **Ca** with the ethanol ligand in the *trans*-position to the pyridine ring is slightly lower in energy than **Cb** having the ethanol ligand in

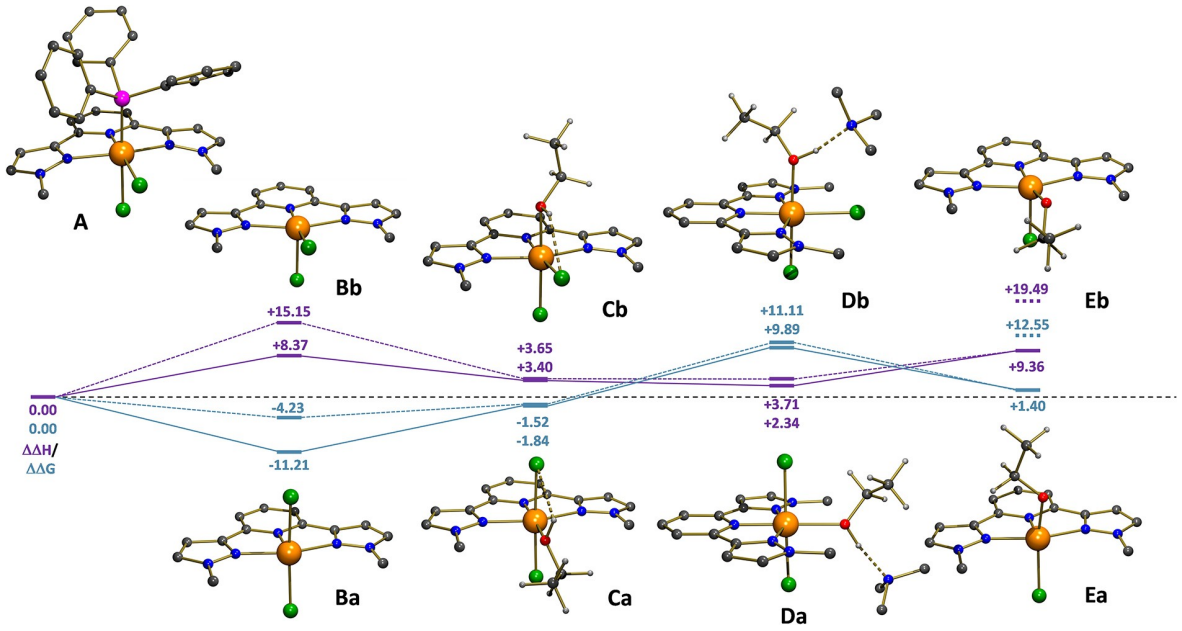

Figure 1. Catalyst activation: calculated molecular structures and energies; all energies in kcal/mol; full lines connect isomer **Ba** and the following intermediates, dashed lines connect isomer **Bb** and the following intermediates; ΔΔH values are given in violet, ΔΔG values in blue; enlarged drawings of the molecular structures are depicted in the Supporting Information.

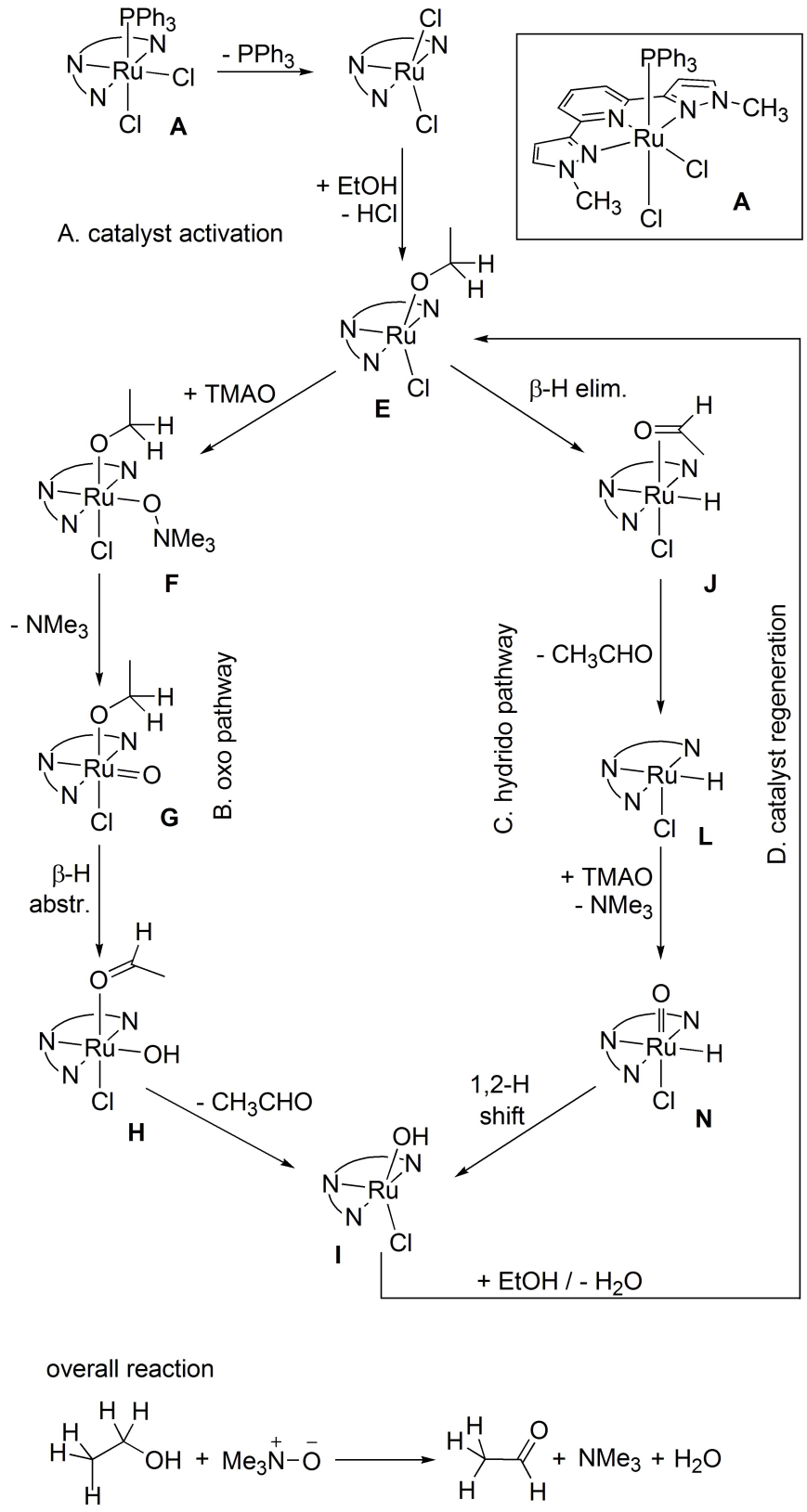

Scheme 3. Summary of the calculated reaction mechanism including *catalyst activation and regeneration* and two alternative pathways for the oxygen transfer (*oxo and hydrido pathways*). The labelling of the species (**A**-N) refers to the discussion below. To allow a straightforward overview on the mechanism, a series of intermediates, other stereoisomers and all calculated transition states are omitted. Bottom: Reaction equation summing up the oxidation of ethanol to acetaldehyde with TMAO as the oxygen source.

the *cis*-position to pyridine. An alternative sequence wherein ethanol is deprotonated prior to the addition to the ruthenium (II) site might be possible, too. However, we believe, that according to the low acidity of ethanol and the rather low basicity of the bases trimethylamine and trimethylamine *N*-oxide, the ethanolate concentration in the solution is not high enough for this pathway. By coordination to the ruthenium(II) site, the acidity of ethanol will increase by several orders of magnitude. Elimination of HCl from the intermediate ethanol adduct was calculated with one molecule of trimethylamine as the base.

In the real catalytic system, the base requested for the elimination of HCl can either be TMAO or NMe_3. Their concentrations will change during the course of the reaction. We therefore have investigated the interaction between the weaker base TMAO and a primary alcohol (here *n*-propanol) in DMF solutions with molecular dynamics simulations (for details see the Supporting Information). The analysis of the local concentrations of TMAO around the alcohol from the simulation results reveals a high affinity between the oxygen atom of TMAO and the proton of the alcohol OH group, even at low concentrations of TMAO. These results support both hypotheses: TMAO can act as a base in the early state of the transformation (low NMe_3 concentration) and an excess of TMAO is beneficial.

The reaction enthalpy $\Delta\Delta H$ for the formation of the hydrogen bound trimethylamine adducts **Da** and **Db** is close to 0.0 kcal/mol, while the final 16VE chloridoethanolatoruthenium (II) complex **Ea** is comparable in its $\Delta\Delta G$ value with the dichlorido complex **A.** **Ea** has a *trans*-orientation of the ethanolato and the chlorido ligand. However, there are two other possible isomers having the ethanolato and the chlorido ligand in *cis*-orientation to each other, one with the ethanolato ligand *trans* to the pyridine ring (**Eb**), the other with the chlorido ligand *trans* to pyridine (not shown in Figure 1). The latter was not included in the calculations, since this geometry prevents the transformation of the ethanolato ligand in both of the following steps (see below). Calculations showed that **Eb** is by more than 11 kcal/mol higher in energy than **Ea**. Calculation of the equilibrium constant for the reaction **Ea** $\rightleftharpoons$ **Eb** by taking the ΔG values of the two isomers gives $K = 6.37 \cdot 10^6$. In a first summary, the energy requested for the formation of the chloridoethanolatoruthenium(II) complex **Ea** from the dichloridotriphenylphosphine)ruthenium(II) complex **A** is low.

Oxo pathway. The early formation of an oxoruthenium(IV) intermediate is the central step of the oxo pathway. It starts from **Ea** resp. **Eb** (Figure 2). The addition of TMAO to these intermediates is as expected endergonic (ΔG) due to the bond formation but almost thermoneutral with respect to ΔH. Isomer **Fb** having the TMAO ligand in the *trans*-position to the chlorido

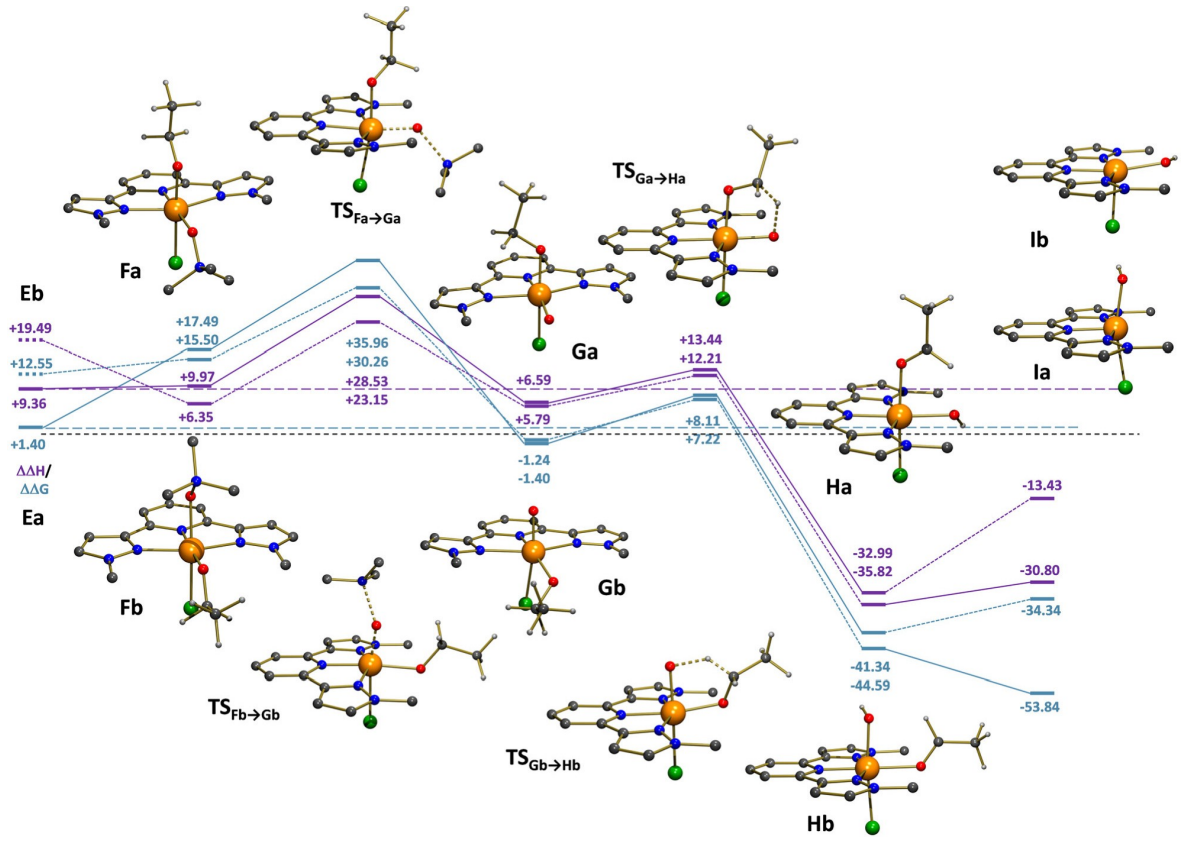

Figure 2. Oxo pathway: calculated molecular structures and energies; all energies in kcal/mol; full lines connect isomer **Ea** and the following intermediates, dashed lines connect isomer **Eb** and the following intermediates; $\Delta\Delta H$ values are given in violet, $\Delta\Delta G$ values in blue; enlarged drawings of the molecular structures are depicted in the Supporting Information.

ligand is slightly more stable than the isomer **Fa** with the TMAO ligand in the *trans*-position to the pyridine site. This can be explained by the fact that chloride is a poorer σ-donor than pyridine. The following two transition states $\mathbf{TS_{Fa\rightarrow Ga}}$ and $\mathbf{TS_{Fb\rightarrow Gb}}$ leading to the formation of the oxoruthenium(IV) intermediates **Ga** and **Gb** are by about 15–17 ($\Delta G^{\ddagger}$) resp. 17–19 kcal/mol ($\Delta H^{\ddagger}$) higher in energy than their precursors **Fa** and **Fb**. Each of these values is not too high to fit well to the rapid catalytic conversions we observe at 80 °C. The two resulting isomeric 18VE chloridoethanolatooxoruthenium(IV) products **Ga** and **Gb** are considerably lower in energy than complex **Ea**, the sequence starts with. The next step, the intermolecular transfer of a hydride from the ethanolato to the oxo ligand via the two cyclic, five-membered transition states $\mathbf{TS_{Ga\rightarrow Ha}}$ and $\mathbf{TS_{Gb\rightarrow Hb}}$ should also proceed rapidly, since the according barriers for both isomers are very low. Two isomeric chloridohydroxidoruthenium(II) complexes **Ha** and **Hb** each containing a σ-bound acetaldehyde ligand are formed in a strongly exothermal and exergonic reaction. The according isomers having π-bound acetaldehyde ligands were not calculated. Due to the results shown in the hydrido pathway (see below), we expect them to be slightly lower in energy than the σ-bound isomers. Dissociation of acetaldehyde results in the formation of a chloridohydroxidoruthenium(II) complex again existing as three stereoisomers. The stereoisomer **Ia** with the chlorido and the hydroxido ligand in *trans*-orientation to each other and the stereoisomer **Ib** with the hydroxido ligand in *trans*-position to the pyridine site were included in the calculations. The latter is much higher in energy than the first one, which therefore is the compound, that the catalyst regeneration sequence starts with (see below) The stereoisomer with the chlorido ligand in *trans*-position to the pyridine site was not calculated, since the addition of ethanol to this stereoisomer (see catalyst regeneration below) would result in a geometry, where the intramolecular transfer of a proton from the ethanol ligand to the hydroxido ligand is not possible.

Hydrido pathway. In the hydrido pathway, a hydridoruthenium(II) complex is generated prior to the oxidation of the ruthenium site (Figure 3). It starts with a β-hydride elimination from the ethanolato ligand in **Ea** (see Figure 1) leading to the hydridoruthenium(II) complex **Ja** bearing a π-coordinated acetaldehyde moiety in the *trans*-position to the chlorido ligand. The $\Delta\Delta G^{\ddagger}$ value for the according transition state $\mathbf{TS_{Ea\rightarrow Ja}}$ was calculated to be 11.46 kcal/mol higher than ΔΔG of the starting compound **Ea**. An alternative pathway starting from isomer **Eb** with the ethanolato ligand in the *trans*-position to the pyridine site (not shown in Figure 3) is energetically not feasible. This process would lead to a hydridoruthenium(II) complex with a π-coordinated acetaldehyde moiety in *trans*-position to the pyridine site and the hydrido ligand in *trans*-position to the chlorido ligand. By scanning the reaction coordinate of this mode of hydride transfer, we found a local

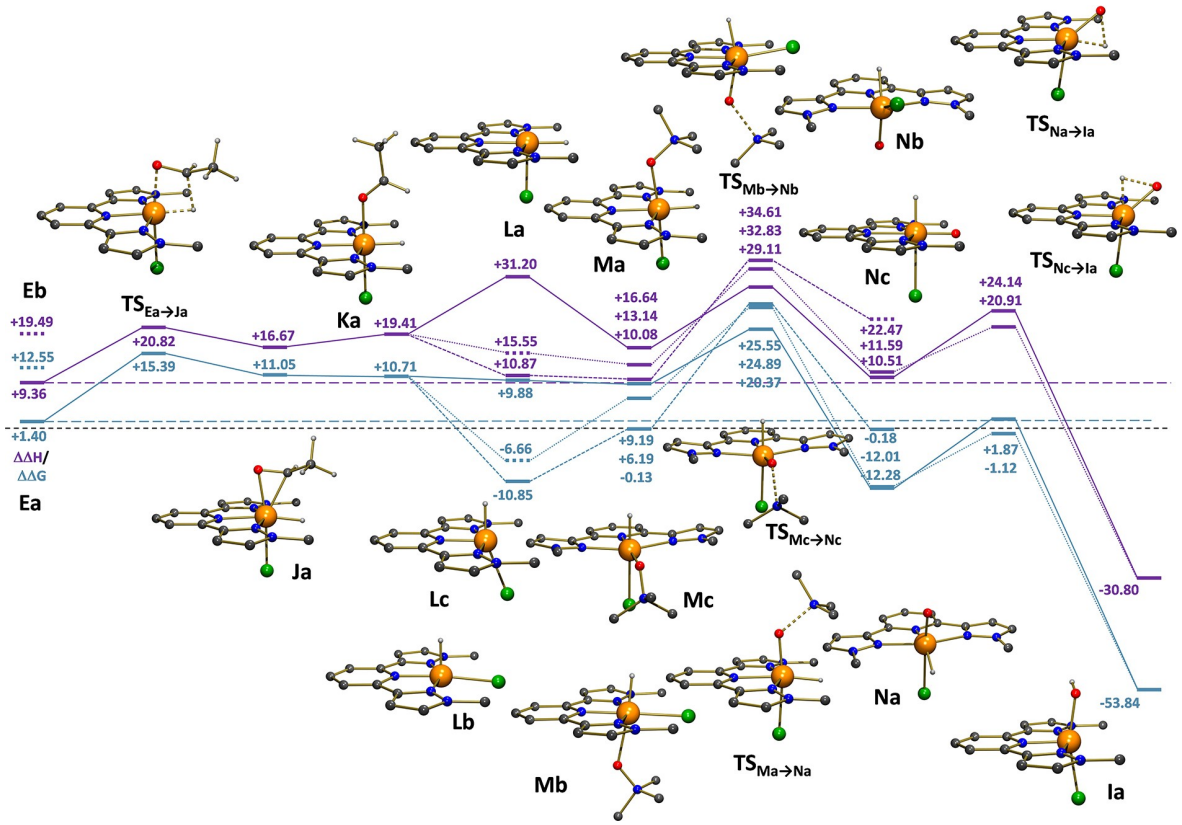

Figure 3. Hydrido pathway: calculated molecular structures and energies; all energies in kcal/mol; full lines connect isomer **Ea** and the following intermediates, dashed and dotted lines connect other structurally related isomers; ΔΔH values are given in violet, ΔΔG values in blue; enlarged drawings of the molecular structures are depicted in the Supporting Information.

minimum for a complex with a strong β-agostic Ru–H interaction that is connected to the starting geometry with a local transition state. However, a further approach of the β-hydrogen atom to the ruthenium(II) center does not lead to the desired formation of a π-coordinated acetaldehyde ligand. Probably this route is not possible due to steric reasons that prevent the acetaldehyde to coordinate in the position between the two *N*-methyl groups. The reaction therefore proceeds via complex **Ka**, wherein the acetaldehyde is now σ-coordinated to the ruthenium(II) site. ΔΔH for **Ja**→**Ka** is slightly positive while ΔΔG is slightly negative, which matches the larger degree of freedom of the σ-coordinated compared to the π-coordinated acetaldehyde ligand. Dissociation of acetaldehyde generates chloridohydridoruthenium(II) complexes, which can appear in three isomeric structures: a) **La**, wherein the hydrido ligand is coordinated in the *trans*-position to the pyridine donor, b) **Lb**, wherein the chlorido ligand is found in the *trans*-position to the pyridine donor, and c) **Lc** with the hydrido and the chlorido ligand being in *trans*-orientation to each other. Isomer **Lc** is not a stable minimum on the energy hypersurface and relaxes either to **La** or to **Lb**. However, the energy that is required to bring the chlorido and the hydrido ligand in *trans*-orientation to each other is only about 5 kcal/mol higher in energy than **Lb**. This result was obtained by scanning the according coordinate (angle Cl–Ru–H). **Lb** is energetically largely favored over **La** (ΔΔH: 21.32, ΔΔG: 21.72 kcal/mol), which can be explained by the high σ-donor strength of the hydrido ligand, preferring no strong σ-donor in the *trans*-position. These two isomers directly provide a free site for the coordination of TMAO, which leads to the six-coordinated ruthenium(II) complexes **Ma** and **Mb**. This addition is strongly exothermal for **La**→**Ma** and endergonic for **Lb**→**Mb** which is due to the *trans*-influence of the hydrido ligand. However, we also included the third isomer **Mc** (TMAO *trans* to pyridine) into our calculations since the orientation of the ligands in **Mb** does not give access to a hydrido ligand in *cis*-orientation to an oxo ligand. Loss of NMe_3 produces the corresponding chloridohydridooxoruthenium(IV) species **Na-Nc**. The three according transition states $\mathbf{TS_{Ma\rightarrow Na}}$-$\mathbf{TS_{Mc\rightarrow Nc}}$ are by $\Delta\Delta H^{\neq} = 34.6\text{-}29.11$ kcal/mol higher in enthalpy than **Ma–Mc**. The chloridohydridooxoruthenium(II) intermediates **Na-Nc** differ largely in their energies. According to the strong *trans*-influences of both, the hydrido and the oxo ligand, intermediate **Nb** is energetically unfavorable since these two ligands are oriented in *trans*-position to each other. In addition, this is the only orientation of the oxo and hydrido ligand that does not allow a direct insertion of the oxo ligand into the Ru–H bond, which will occur in the following step. However, instead of being a "dead end" of the reaction sequence, **Nb** might be converted into **Na** or **Nc** by dissociation of the chlorido ligand and its re-coordination in an appropriate orientation. The energetics of this process was not calculated. The barriers related to the two transition states $\mathbf{TS_{Na\rightarrow Ia}}$ and $\mathbf{TS_{Nc\rightarrow Ia}}$ are rather low. Interestingly, the oxo ligand moves to the hydrido ligand and not vice versa. Species **Ia** is identical to the final compound of the Ru=O pathway as described above. For a second isomer **Ib** see the discussion above (oxo pathway).

Catalyst regeneration. Both, the oxo and the hydrido pathway end up with the chloridohydroxidoruthenium(II) complexes **Ia** and **Ib**. In the final part of the reaction sequence, the catalyst regeneration (Figure 4), the hydroxido ligand has to be exchanged against an ethanolato ligand leading back to the central chloridoethanolatoruthenium(II) intermediates **Ea** and

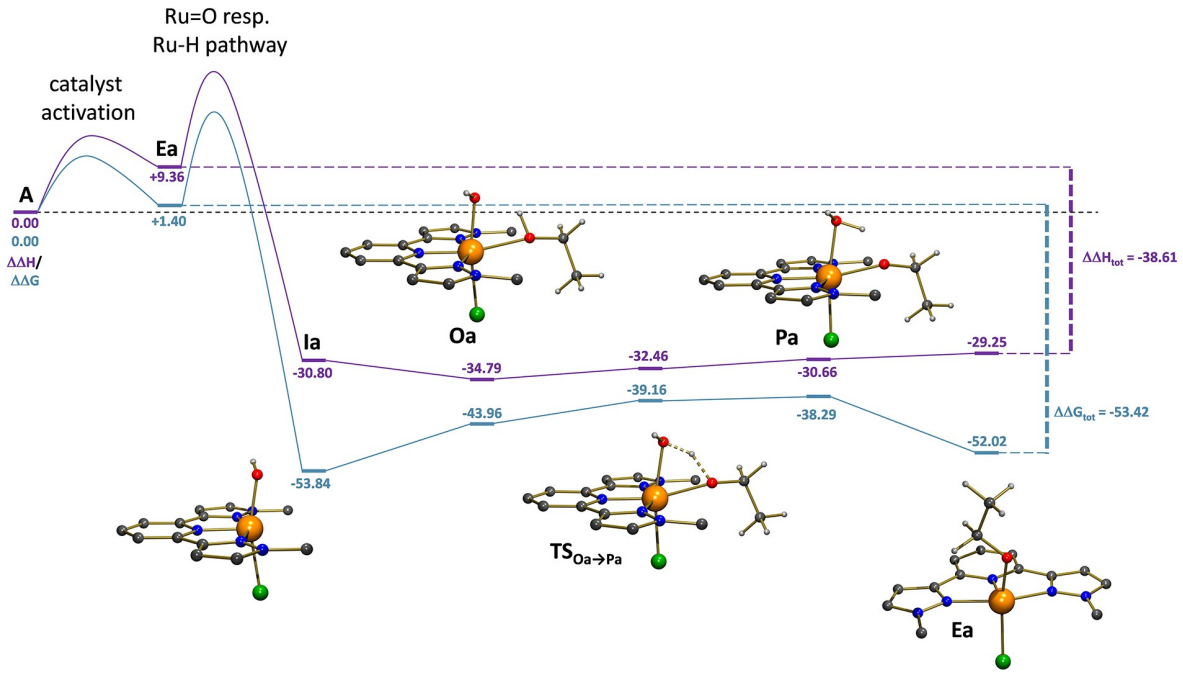

Figure 4. Catalyst regeneration pathway: calculated molecular structures and energies; all energies in kcal/mol; ΔΔH values are given in violet, ΔΔG values in blue; enlarged drawings of the molecular structures are depicted in the Supporting Information.

Eb from which the oxo and the hydrido pathway started. Since the energetic differences between the isomers from the a- and the b-series are small, only the a-series was calculated here. Addition of ethanol to the 16VE complex **Ia** gives the 18 VE intermediate **Oa**, in a slightly exothermal but endergonic reaction. The hydrogen bond formed between the ethanol OH group and the oxygen atom of the hydroxo ligand paves the way for the generation of an ethanolato and a water ligand which proceeds via the low laying transition state $\mathbf{TS_{Oa->Pa}}$. The energetic data given for the resulting aquachloridoethanolatoruthenium(II) complex **Pa** are slightly higher than for $\mathbf{TS_{Oa->Pa}}$, which is contradictory at a first glance. However, the computational optimization of the structures is done on the E hypersurface and an imaginary frequency prove that $\mathbf{TS_{Oa->Pa}}$ is really a transition state. Dissociation of water in an almost thermoneutral reaction regenerates **Ea**.

At the moment, there is no experimental evidence for one of the species discussed above, despite the equilibrium of phosphine dissociation, the sequence starts with. However, oxidoruthenium(IV) species have been postulated as intermediates in water oxidation processes.[14]

In addition to the calculations discussed above, we also investigated four alternatives for a direct transfer of a hydrogen atom to TMAO, which avoid the oxidation to ruthenium(IV): On one side the hydrogen abstraction from the ethanolato ligand of the chloridoethanolatoruthenium(II) complex **Ea** or from the chloridohydridoruthenium(II) complex **Lc** by uncoordinated TMAO. On the other side the direct transfer of a hydrogen atom to TMAO in complexes Ma and Ga (for a graphical explanation see the Supporting Information). No transition states could be located for these reactions by using the QST2 or QST3 keyword in the GAUSSIAN optimization. Additional attempts to localize the transition state by performing scans along the critical reaction coordinates also failed. The energies of these calculations raised far above those of the highest transition states found for the two pathways discussed above. This can be explained by the charges of the hydrogen atom that is transferred and the oxygen atom at TMAO that has to accept this hydrogen atom. Both are negatively polarized, they are nucleophiles. Or in other words: the oxygen atom only gains sufficient electrophilicity (oxenoid character) when it has lost the NMe_3 moiety and is coordinated as an oxido ligand to ruthenium(IV).

On the basis of the DFT calculations, it is not possible to decide whether the hydrido or the oxo pathway is the route that leads to the product. The barrier of the oxo pathway is at $\Delta\Delta G^{\neq} = 30.26$ and $\Delta\Delta H^{\neq} = 23.15$ kcal/mol for $\mathbf{TS_{Fb\rightarrow Gb}}$, the highest barrier of the hydrido pathway is at $\Delta\Delta G^{\neq} = 20.37$ and $\Delta\Delta H^{\neq} = 29.11$ kcal/mol for $\mathbf{TS_{Ma\rightarrow Na}}$ with respect to compound A. So in terms of the free energy the hydrido pathway should be the preferred route, in terms of enthalpy it's the oxo pathway. However, the low barriers of activation found here make clear, that high oxidation state ruthenium species may not necessarily be required for this type of oxidation. In classical transfer hydrogenation reactions, M–H intermediates are formed. Therefore, at least a part of the hydride route fits to the proposal of Sharpless et al., that the ruthenium catalysed oxidation of alcohols with *N*-oxides as the oxygen source can be considered as something like a reversion of a hydrogenation reaction.

Conclusions

We here have reported two easily applicable and highly efficient ways to use the ruthenium catalysed Griffith-Ley oxidation for the generation of a wide variety of aldehydes and ketones with very low catalyst loadings at short reaction times. The use of a nonpolar solvent that dissolves the alcohol and the product but not the catalyst and the oxygen source, which then form a second polar phase together with a part of the alcohol can be taken as a paradigm for other (oxidation) reactions. In addition, quantum chemical calculations showed that at least for catalyst **1**, there are alternative pathways for the Griffith-Ley oxidation that do not require ruthenium in high oxidation states but involve ruthenium species in the oxidation states +II and +IV. Based on these calculations we can propose two possible mechanisms proceeding with ruthenium species in the oxidation states +II and +IV, that differ in the order of the oxygen and hydrogen transfer steps. Oxidoruthenium(IV) intermediates take part in this process, which are reduced back to ruthenium(II) by hydride transfer. The direct transfer of a hydride to TMAO, either coordinated or un-coordinated is energetically unfavourable. We believe that our results fit well to the role that is addressed to oxoruthenium(IV) species in the water oxidation and maybe will enhance the interest in deeper investigations on other oxidation processes with this element.

Experimental Section

General information: Purification and drying of solvents was carried out according to standard methods. Synthesis and catalysis were performed under an atmosphere of nitrogen although the ruthenium catalysts are not sensitive towards oxygen and moisture. References and NMR data belonging to the synthesis of compound **1** are deposited in the Supporting Information.

Catalytic reactions. All catalytic experiments were performed in crimp top vials purchased from VWR International GmbH with a total volume of 20 mL. The catalyst and TMAO were weighed and filled in the vials, a magnet stirrer was added and the vials were sealed with ptfe septa followed by three cycles of 15 min of evacuation and purging with dry nitrogen. Solvent and internal standard were added by use of syringes. The vials were placed in an aluminum heating block with normed boreholes preheated to the reaction temperature. Then the substrate was added by use of a syringe. Samples were taken with single use syringes and cannula (Braun GmbH) and were analyzed with a Clarus 580 GC equipped with a FID-detector or a Varian 3900 GC-MS (2100T). GC columns: FS-OV-1701-CB-0.25 (30 m, d = 0.25 mm, CS Chromatographie Service GmbH).

Hazard note: Leaving the solvent and carrying out the experiments with the alcohol as the only liquid component led to explosions of the vials! Even when an excess of alcohol was used and the vial is not closed, the mixtures started to burn heavily after some seconds of initialization.

Quantum chemical calculations: The calculations on the mechanism of the oxidation of alcohols to ketones and aldehydes were carried out with the program Gaussian16[15] using the B3LYP gradient corrected exchange-correlation functional[16] in combination with the 6–31 + G* basis set for C, H, N, O, Cl[17] obtained from the EMSL/PNNL Basis Set Exchange site.[18] For ruthenium, the according Stuttgart RSC 1997 ECP basis set was applied.[19] The influence of the solvent DMF was included in the calculations by performing PCM calculations using the CPCM polarizable conductor calculation model.[20] Temperature was set to 358.15 K (85 °C). Full geometry optimizations were carried out in C_1 symmetry using analytical gradient techniques and the resulting structures were confirmed to be true minima by diagonalization of the analytical Hessian Matrix. The thermodynamic corrections were obtained from the frequency calculations. In most cases scans along the internal reaction coordinate were carried out to locate the transition state. The starting geometry of compound **1** for the calculations was taken from a solid-state structure.

Acknowledgements

The authors gratefully acknowledge financial support by the EU-INTERREG project BIOVAL.

Conflict of Interest

The authors declare no conflict of interest.

Keywords: alcohol · oxidation · ruthenium · mechanism · DFT calculation

[1] a) J. R. Holum, *J. Org. Chem.* **1961**, *26*, 4814–4816; b) J. C. Collins, W. W. Hess, J. Frank, *Tetrahedron Lett.*, **1968**, *30*, 3363–3366; c) R. Ratcliffe, R. Rodehorst, *J. Org. Chem.* **1970**, *35*, 4000–4002; d) D. G. Lee, U. A. Spitzer, *J. Org. Chem.* **1970**, *35*, 3589–3590; e) K. B. Sharpless, K. Akashi, *J. Am. Chem. Soc.* **1975**, *97*, 5927–5928; f) F. A. Luzzio, *Org. React.* **1998**, *53*, 1–221; g) J.-D. Lou, Z.-N. Xu, *Tetrahedron Lett.* **2002**, *43*, 6095–6097; h) D. L. Turner, *J. Am. Chem. Soc.* **1954**, *76*, 5175–5176; i) F. M. Menger, C. Lee, *J. Org. Chem.* **1979**, *44*, 3446–3448.

[2] a) W. P. Griffith, S. V. Ley, G. P. Whitcombe, A. D. White, *J. Chem. Soc. Chem. Commun.* **1987**, *21*, 1625–1627; b) W. P. Griffith, *Plat. Met. Rev.* **1989**, *33*, 181–185; c) W. P. Griffith, *Chem. Soc. Rev.* **1992**, *21*, 179–185.

[3] a) P. W. Moore, C. D. G. Read, P. V. Bernhardt, C. M. Williams, *Chem. Eur. J.* **2018**, *24*, 4556–4561; b) P. W. Moore, Y. Jiao, P. M. Mirzayans, L. N. Q. Sheng, J. P. Hooker, C. M. Williams, *Eur. J. Org. Chem.* **2016**, 3401–3407; c) C. D. G. Read, P. W. Moore, C. M. Williams, *Green Chem.*, **2015**, *17*, 4537–4540; d) P. W. Moore, P. M. Mirzayans, C. M. Williams, *Chem. Eur. J.* **2015**, *21*, 3567–3571; e) J. A. Caturelli Kuran, A. G. Moglioni, *Synth. Commun.* **2014**, *44*, 2393–2400; f) S. I. Murahashi, N. Komiya, in *Modern Oxidation Methods*, 2nd ed. (Ed.: J.-E. Baeckvall), Wiley-VCH, Weinheim, **2010**, pp. 241–275; g) B.-Z. Zhan, A. Thompson, *Tetrahedron* **2004**, *60*, 2917–2935.

[4] a) K. B. Sharpless, K. Akashi, K. Oshima, *Tetrahedron Lett.* **1976**, *29*, 2503–2506; b) E. Duliere, B. Tinant, A. Schanck, M. Devillers, J. Marchand-Brynaert, *Inorg. Chim. Acta* **2000**, *311*, 147–151.

[5] M. L. S. Almeida, M. Beller, G.-Z. Wang, J.-E. Backvall, *Chem. Eur. J.* **1996**, *2*, 1533–1536.

[6] a) T. J. Zerk, P. W. Moore, C. M. Williams, P. V. Bernhardt, *Chem. Commun.* **2016**, *52*, 10301–10304; b) T. J. Zerk, P. W. Moore, J. S. Harbort, S. Chow, L. Byrne, G. A. Koutsantonis, J. R. Harmer, M. Martinez, C. M. Williams, P. V. Bernhardt, *Chem. Sci.* **2017**, *8*, 8435–8442; c) P. W. Moore, T. J. Zerk, J. M. Burns, P. V. Bernhardt, C. M. Williams, *Eur. J. Org. Chem.* **2019**, 303–308.

[7] a) Y. Shvo, E. Hazum, *J. Chem. Soc. Chem. Commun.* **1974**, 336–337; b) D. J. Blumer, K. W. Barnett, T. L. Brown, *J. Organomet. Chem.* **1979**, *173*, 71–76; c) T. Y. Luh, C. S. Wong, *J. Organomet. Chem.* **1985**, *287*, 231–233; d) H. Fischer, S. Zeuner, K. Ackermann, J. Schmid, *Chem. Ber.* **1986**, *119*, 1546–1556.

[8] P. Capdevielle, D. Sparfel, J. Baranne-Lafont, C. Nguyen Kim, M. Maumy, *J. Chem. Soc. Chem. Commun.* **1990**, *7*, 565–566.

[9] B. Hinzen, S. V. Ley, *J. Chem. Soc. Perkin Trans. 1* **1997**, 1907–1908.

[10] a) A. J. Pearson, Y. Kwak, *Tetrahedron Lett.* **2005**, *46*, 5417–5419; b) A. J. Pearson, Y. Kwak, *Tetrahedron Lett.* **2005**, *46*, 3407–3410.

[11] E. R. Klobukowski, R. J. Angelici, L. K. Woo, *Catal. Lett.* **2012**, *142*, 161–167.

[12] J. A. Soderquist, C. L. Anderson, *Tetrahedron Lett.* **1986**, *27*, 3961–3962.

[13] a) L. Taghizadeh Ghoochany, S. Farsadpour, Y. Sun, W. R. Thiel, *Eur. J. Inorg. Chem.* **2011**, 3431–3437; b) P. Weingart, W. R. Thiel, *ChemCatChem* **2018**, *10*, 4844–4848.

[14] a) J. K. Hurst, *Coord. Chem. Rev.* **2005**, *249*, 313–328; b) D. W. Shaffer, Y. Xie, J. J. Concepcion, *Chem. Soc. Rev.* **2017**, *46*, 6170–6193; c) J. J. Concepcion, J. W. Jurss, M. K. Brennaman, P. G. Hoertz, A. Otávio, T. Patrocinio, N. Y. Murakami Iha, J. L. Templeton, T. J. Meyer, *Acc. Chem. Res.* **2009**, *42*, 1954–1965.

[15] M. J. Frisch, G. W. Trucks, H. B. Schlegel, G. E. Scuseria, M. A. Robb, J. R. Cheeseman, G. Scalmani, V. Barone, G. A. Petersson, H. Nakatsuji, X. Li, M. Caricato, A. V. Marenich, J. Bloino, B. G. Janesko, R. Gomperts, B. Mennucci, H. P. Hratchian, J. V. Ortiz, A. F. Izmaylov, J. L. Sonnenberg, D. Williams-Young, F. Ding, F. Lipparini, F. Egidi, J. Goings, B. Peng, A. Petrone, T. Henderson, D. Ranasinghe, V. G. Zakrzewski, J. Gao, N. Rega, G. Zheng, W. Liang, M. Hada, M. Ehara, K. Toyota, R. Fukuda, J. Hasegawa, M. Ishida, T. Nakajima, Y. Honda, O. Kitao, H. Nakai, T. Vreven, K. Throssell, J. A. Montgomery, Jr., J. E. Peralta, F. Ogliaro, M. J. Bearpark, J. J. Heyd, E. N. Brothers, K. N. Kudin, V. N. Staroverov, T. A. Keith, R. Kobayashi, J. Normand, K. Raghavachari, A. P. Rendell, J. C. Burant, S. S. Iyengar, J. Tomasi, M. Cossi, J. M. Millam, M. Klene, C. Adamo, R. Cammi, J. W. Ochterski, R. L. Martin, K. Morokuma, O. Farkas, J. B. Foresman, and D. J. Fox, Gaussian, Inc., Wallingford CT, 2016.

[16] a) P. J. Stephens, F. J. Devlin, C. F. Chabalowski, M. J. Frisch, *J. Phys. Chem.* **1994**, *98*, 11623–11627; b) A. D. Becke, *J. Chem. Phys.* **1993**, *98*, 5648–5652; c) A. D. Becke, *Phys. Rev. A*, **1988**, *38*, 3098–3100; d) C. Lee, W. Yang and R. G. Parr, *Phys. Rev. B*, **1988**, *37*, 785–789.

[17] a) P. C. Hariharan, J. A. Pople, *Theoret. Chim. Acta* **1973**, *28*, 213–222; b) M. M. Francl, W. J. Petro, W. J. Hehre, J. S. Binkley, M. S. Gordon, D. J. DeFrees, J. A. Pople, *J. Chem. Phys.* **1982**, *77*, 3654–3665; c) T. Clark, J. Chandrasekhar, G. W. Spitznagel, P. v. R. Schleyer, *J. Comb. Chem.* **1983**, *4*, 294–301; d) R. Krishnam, J. S. Binkley, R. Seeger, J. A. Pople, *J. Chem. Phys.* **1980**, *72*, 650–654.

[18] a) D. Feller, *J. Comb. Chem.* **1996**, *17*, 1571–1586; b) K. L. Schuchardt, B. T. Didier, T. Elsethagen, L. Sun, V. Gurumoorthi, J. Chase, J. Li, T. L. J. Windus, *J. Chem. Inf. Model.* **2007**, *47*, 1045–1052.

[19] a) A. Bergner, M. Dolg, W. Küchle, H. Stoll, H. Preuss, *Mol. Phys.* **1993**, *80*, 1431–1441; b) M. Kaupp, P. v. R. Schleyer, H. Stoll, H. Preuss, *J. Chem. Phys.* **1991**, *94*, 1360–1366.

[20] a) V. Barone, M. Cossi, *J. Phys. Chem. A* **1998**, *102*, 1995–2001; b) M. Cossi, N. Rega, G. Scalmani, V. Barone *J. Comb. Chem.* **2003**, *24*, 669–681.

Manuscript received: March 9, 2020
Revised manuscript received: April 23, 2020
Accepted manuscript online: April 24, 2020
Version of record online: June 16, 2020